JOURNAL OF MECHANICAL ENGINEERING AND SCIENCES
ISSN: 2289-4659 e-ISSN: 2231-8380
VOLUME 19, ISSUE 2, 2025, 10676 - 10684
DOI: https://doi.org/10.15282/jmes.19.2.2025.9.0837

RESEARCH ARTICLE

Influence of laser power and scanning speed on necking growth of SS316L powder in laser melting processes

M. R. Mazlan[1], N. H. Jamadon[1,2*], A. B. Sulong[1,2], F. I. Jamhari[1], M. A. Aripin[1,4], N. A. M. Radzuan[1,2], F. Yusof[3]

[1] Department of Mechanical and Manufacturing Engineering, Faculty of Engineering and Built Environment, Universiti Kebangsaan Malaysia, 43600 Bangi, Selangor, Malaysia

Phone: +60389216418, Fax: +60389252546

[2] Centre for Materials Engineering and Smart Manufacturing (MERCU), Department of Mechanical and Manufacturing Engineering, Faculty of Engineering & Built Environment, Universiti Kebangsaan Malaysia, 43600 Bangi, Selangor, Malaysia

[3] Department of Mechanical Engineering, Faculty of Engineering, University of Malaya, Jalan Professor Diraja Ungku Aziz, 50603 Kuala Lumpur, Malaysia

[4] Department of Mechanical Engineering, Faculty of Engineering, City University, 46100, Petaling Jaya, Selangor, Malaysia

ABSTRACT - Necking is a crucial phenomenon that can highly affect the mechanical properties and structural integrity of the material, especially in additive manufacturing. To understand the effect of laser power and scanning speed on necking formation between powder particles for SS316L, a study was conducted on the joining of powder particles under various laser parameters. This knowledge is valuable for fine-tuning laser processing parameters across various industrial applications. For this study, Uniweld Laser 3000 was used for the laser joining process. For the laser parameters, laser speeds ranging from 50 mm/s to 150 mm/s and laser powers of 15 W, 20 W, and 25 W were used in this study. The laser process was concentrated explicitly on observing the powder joining process within a single track. It was observed that the necking size increases as the laser power increases and the scanning speed decreases. At 150 mm/s with 150 W, no particle joining was observed as the powder absorbed insufficient energy to undergo the melting process. At different laser powers, the necking growth rate between scanning speeds varies. When laser power was 15 W and scanning speed was 125 mm/s, the neck size increased to 49 µm. The necking increases further to 62 µm, 93 µm, and 100 µm when the scanning speed is reduced to 100 mm/s, 75 mm/s, and 50 mm/s. The same trend can also be observed under higher laser power, but at a different neck growth rate. Analysis of dislocation density for different laser parameters was also performed. It has been found that the highest energy density corresponds to the highest dislocation density, with a value of 2.03×10^{14} m^{-2}. It can be concluded that a slower scanning speed allows particles to absorb more heat for the melting process, hence increasing the necking size of the particles.

ARTICLE HISTORY
Received : 21st Oct. 2024
Revised : 06th May 2025
Accepted : 11th June 2025
Published : 30th June 2025

KEYWORDS
Particle joining
Powder diffusion
Necking
SLM
Laser parameter

1. INTRODUCTION

In recent years, manufacturing has evolved from traditional subtractive manufacturing processes to formative manufacturing processes. Initially, subtractive manufacturing techniques such as turning, milling, and drilling were widely used for production [1]. However, these techniques face a few challenges, especially when cutting tough materials such as titanium [2]. To mitigate tool wear, additional coatings were often required on cutting tools [3]. Another major drawback of subtractive manufacturing is the substantial material wastage involved. Therefore, to address this limitation, formative manufacturing processes, such as sand casting, were introduced [4]. Although the formative manufacturing process is efficient and produces less waste, the design of these processes is limited when it comes to complex shapes due to constraints in mold design. Hence, additive manufacturing (AM) was introduced to overcome the limitations of subtractive and formative manufacturing processes. AM is a process in which material is produced layer by layer, resulting in little to no material waste [4, 5]. AM processes are widely used in various sectors, including medical applications, aerospace, and others. This is due to its ability to produce precise and complex shapes [6, 7]. Therefore, one of the well-known processes in AM is Selective Laser Melting (SLM). SLM is a process where a high-energy laser is used to heat powder particles on a bed plate. Then, the powders will absorb enough heat to melt and fuse with neighboring particles layer by layer, until they produce a complete 3D product [8, 9]. Thus, in SLM, the most used materials are stainless steel and titanium. To ensure a stable melting process for these materials, precise control of laser parameters, such as laser power and scan speed, is required. Precise control of laser parameters is necessary to avoid trapped porosity, which is caused by Ostwald ripening. This phenomenon was caused by uneven heating and the melting process [10]. Therefore, neck formation in SLM is a critical factor that needs to be considered. These necks are formed as a result of the melting between two particles, which is crucial for achieving a product with strong interparticle bonding [11, 12].

***CORRESPONDING AUTHOR | N. H. Jamadon** | ✉ nashrahhani@ukm.edu.my

Recently, research on SLM has mainly focused on optimizing the laser parameters, specifically the laser power and scanning speed [13, 14]. However, the formation of these necks during the melting process is also influenced by the powder characteristics, such as the size, shape, and size distribution of the powder. One of the most used materials in SLM processes, other than titanium, is SS316L. SS316L is well known for its high corrosion resistance and excellent mechanical properties, making it very suitable for applications in marine environments, aerospace, and medical fields.

During neck formation, the powder particles joining undergo three different diffusion stages: surface diffusion (SD), volume diffusion (VD), and grain boundary diffusion (GBD). Initially, SD stages occur at early stages where a low energy barrier is required and sufficient to break down the atoms at the particle surface. This causes the powder particles to partially melt, with the surface particles already in a liquid state. Due to the hydrophilic nature of liquid, the melted particles are drawn toward neighbouring particles, forming a liquid bridge known as a neck [15]. The SD stage continues until the neck nearly reaches the size of the particle, at which point the VD stage begins. Compared to SD, the diffusion rate in VD is much slower because more heat is required to overcome the energy barrier and melt the internal portion of the particles. As energy density increases, GBD occurs. Typically, GBD is the final stage in diffusion mechanisms, where it facilitates pore shrinkage and material densification. However, poor thermal stability during the joining process could lead to a poor diffusion process. This could lead to a rapid VD stage, which in turn could result in gas entrapment due to the rapid solidification process. This defect occurs because the GBD diffusion rate is much faster than the VD, where the gas does not have enough time to escape, as GBD takes place much earlier. Hence. Optimising laser parameters is required for proper thermal stability during the neck formation [10].

This study's main focus is on investigating the effects of different laser powers and scanning speeds on neck growth in the SLM process. Besides, this study also aims to determine the strength and melting characteristics of the necks by calculating the dislocation density of the materials. Given the current limitations of SLM machines, the machines are restricted to different types of materials with limited specific parameter settings. Therefore, this study highlights the importance of understanding the neck growth formation for the open SLM system. This understanding would facilitate the utilisation of a broader range of lasers capable of melting or sintering different types of materials.

2. MATERIALS AND METHODS

2.1 Experimental Setup

In this study, the experiment was conducted by using a custom-built chamber equipped with a 1064 nm Theta lens. Figure 1 illustrates the experimental setup for the laser process. Nd: YAG fiber laser with a Gaussian beam profile was used for the laser melting process. The laser beam had a diameter of approximately 150 µm, and the continuous wave mode was employed. To prevent oxidation during the laser process, argon gas was used as the shielding gas. The laser power was set to 15 W, 20 W, and 25 W, while the scanning speed ranged between 50 mm/s and 150 mm/s. Lower laser powers were deliberately selected in this study to facilitate the clear observation of necking between particles, promoting their fusion onto the powder bed and avoiding conditions that would obscure neck formation. In a previous study, a pulsed laser was used instead of a continuous-wave laser to minimize heat absorption by the powder particles [17-18]. To examine the neck formation, the powder was transferred onto copper tape to secure the joined particles. This study focuses on the joining of particles along a single track. A Scanning Electron Microscopy (SEM) machine was used to observe the neck formation, and ImageJ software was employed to measure the average neck size. Particles with a size between 90 and 100 µm were selected for analysis. Table 1 depicts the process parameters used in the single-track experiment.

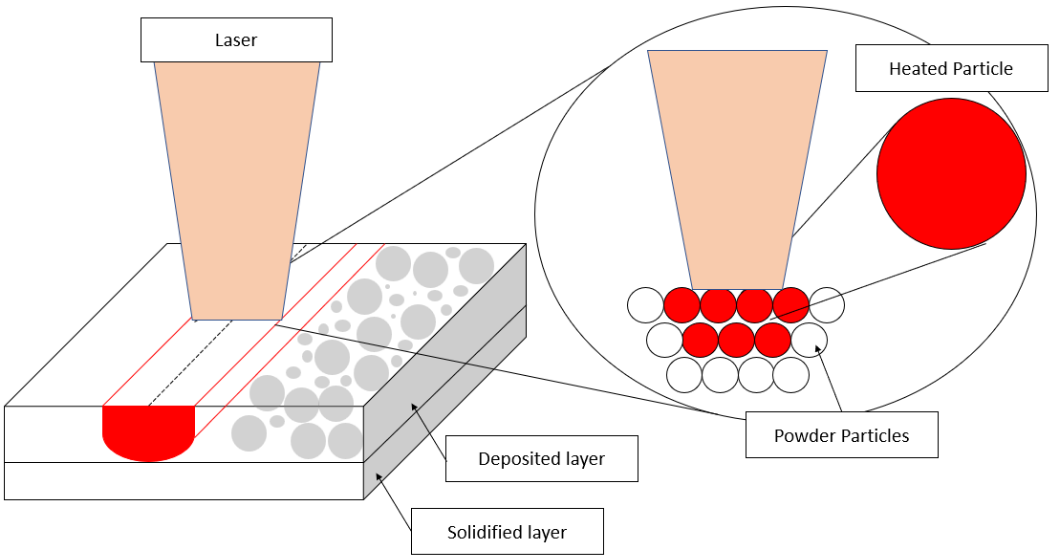

Figure 1. Schematic and parameter setup in laser processing

Table 1. Parameters of the single-track experiment

Sample	Scanning Speed (mm/s)	Laser Power (W)	Particle size (µm)	Laser Type	Laser Process Environment	Laser profile
1	150	15	100	Continuous wave	Argon gas	Gaussian beam
2	125					
3	100					
4	75					
5	50					
6	150	20				
7	125					
8	100					
9	75					
10	50					
11	150	25				
12	125					
13	100					
14	75					
15	50					

2.2 Materials

Gas-atomised SS316L powder with an average size of 100 µm was used in this study. The particle morphology was analysed using a FESEM system (Zeiss, model Merlin Compact from Germany). Figure 2(a) shows the SEM images of gas atomised SS316L. The morphological analysis revealed that the powder consisted of smooth and spherical particles. Compared to irregular shape particles, spherical particles offer more uniform surface areas, which allow for more consistent laser absorption for melting [18]. The spherical morphology is crucial for achieving consistent and reliable sintering outcomes, as it promotes a uniform and homogenous particle structure. Additionally, the spherical shape improves packing density. The particle size distribution is shown in Figure 2(b) and detailed in Table 2 with the average powder size measuring below 100 µm.

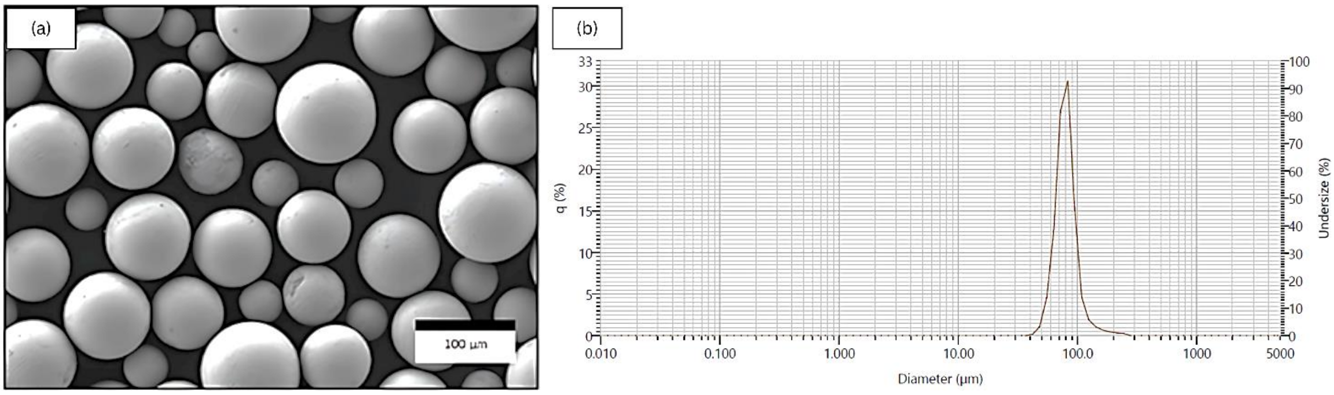

Figure 2. (a) SEM images of gas atomised SS316L with 100 µm diameter and (b) particle size distribution in the SS316L powder

Table 2. Parameters of the single-track experiment

Particle Size Distribution (µm)	D_{10} (µm)	D_{50} (µm)	D_{90} (µm)
100	61.7	79.0	100.6

2.3 Crystallographic Analysis

For crystallographic analysis, X-ray diffraction (XRD) was performed using a Bruker D8 Advance machine at the Research and Instrumentation Center (i-Crim), UKM. The laser-treated powder was adhered to adhesive tape to facilitate the XRD analysis. The sample on the tap was then mounted onto a Perspex glass sheet, chosen for its transparency, which allowed X-rays to penetrate through it and enabled accurate and comprehensive XRD data collection. The adhesive tape did not interfere with the analysis, as XRD primarily detects the dominant material in the sample. The XRD data were subsequently used to calculate the dislocation density of the samples. The Williamson-Hall equation was employed to determine the crystallite size and dislocation density from the XRD data, as shown in Eq. (1).

$$\frac{\beta cos\theta}{\lambda} = \frac{0.9}{D} + 2\varepsilon.\frac{sin\theta}{\lambda} \tag{1}$$

where β is the full width at half maximum (FWHM) of the diffraction peak, and θ is the Bragg diffraction angle. Both FWHM and the Bragg angle can be obtained from the XRD profile, while λ is the X-ray wavelength, which is 0.1542 nm.

Using the same equation, the crystallite size, D, and lattice strain, ε, can be calculated via the linear equation $y = mx + c$, where y represents $\beta cos\theta/\lambda$, m is 2ε, x is $sin\theta/\lambda$, and c is $0.9/D$. The value D *is* then used to calculate the dislocation density, ρ, using Eq. (2).

$$\rho = \frac{2\sqrt{\varepsilon}}{Db} \tag{2}$$

In this equation, ρ denotes the dislocation density, ε is the lattice strain, D is the crystallite size obtained from the linear equation, and b is the Burgers vector (0.254 nm for SS316L austenite).

3. RESULTS AND DISCUSSION

3.1 Neck Size Analysis

To analyse neck growth after the laser process, the samples were observed under SEM, and the neck size was measured using ImageJ. The formation of the neck is highly influenced by the laser scanning speed, as shown in Figure 3. At a laser power of 15 W, no joining or neck was observed at a scanning speed of 150 mm/s, indicating that the energy density was insufficient to overcome the energy barrier and melt the particles. As the speed decreases to 125 mm/s, the formation of a kink with an average size of 49 µm is observed, indicating that the particle partially melts down. At this stage, the most dominant mechanism is SD. As mentioned by Mazlan et al. [10], the SD mechanism is the earliest stage of diffusion, requiring only a small amount of energy to melt and break down the particles at the surface level. At 75 mm/s, the neck size nearly doubled, suggesting that two particles had fully diffused, though irregularities such as surface bumps were still visible, as shown in Figure 3(b). When the scanning speed was further reduced to 50 mm/s, the particles were fully diffused with their neighbouring particles, resulting in a smoother surface, which indicated that stable and complete melting had occurred between the particles.

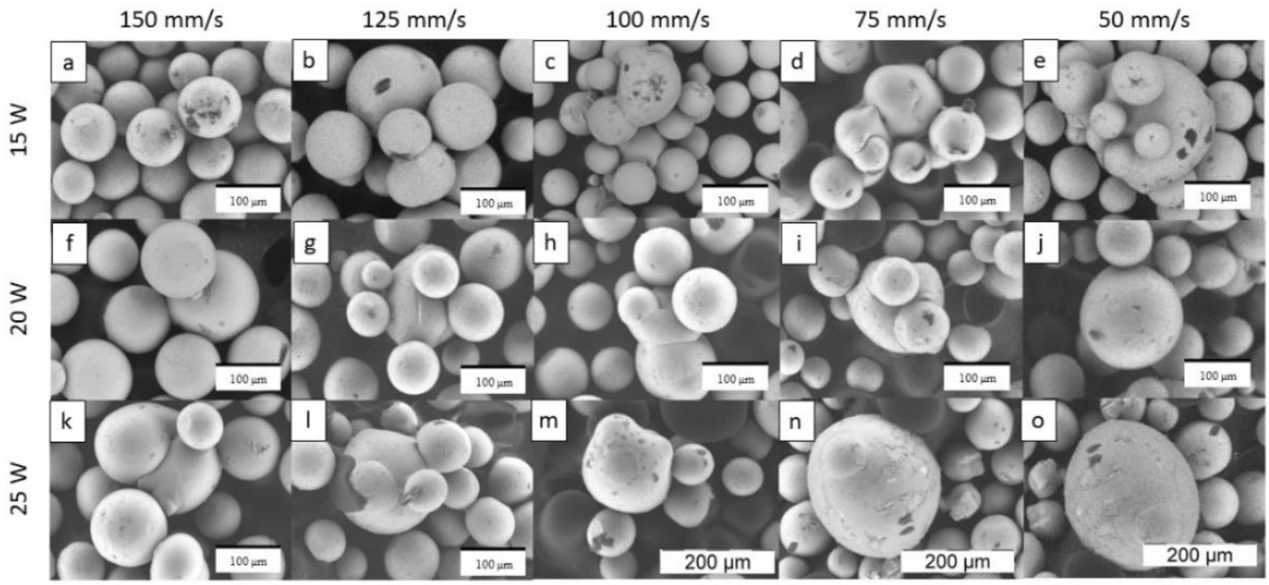

Figure 3. SEM images of joined particles under different laser power and scanning speed

At a laser power of 20 W, kink formation was observed at a scanning speed of 150 mm/s occurring earlier than at 15 W. At this speed, the average neck size is approximately 30.2 µm, indicating that sufficient energy had been absorbed by the particles, allowing the atoms at the surface of particles to melt and diffuse. A further reduction in scanning speed to 125 mm/s resulted in a more pronounced necking, as illustrated in Figure 3(g), with an average neck size of approximately 60 µm. At a speed of 100 mm/s, the neck size increased to approximately 97 µm. At 75 mm/s, the neck size reached 100 µm, indicating full particle diffusion. At this point, the neck was no longer distinguishable, and the particle size had doubled compared to the as-built condition, suggesting significant diffusion but incomplete particle engulfment. Finally, at 50 mm/s, the neck size remained at 100 µm, with the particles fully diffused. The joined particles exhibited a fully smooth surface, indicating complete particle bonding. At the highest laser power of 25 W, the necking process begins even earlier. At 150 mm/s, the average neck size is 45.5 µm. As the scanning speed decreased to 125 mm/s and below, the neck was no longer visible, indicating that particles had fully diffused. However, at 125 mm/s, as shown in Figure 3(l), a large bump was observed on the surface of the powder particles. As the scanning speed was further reduced to 50 mm/s, fewer bumps were seen, as illustrated in Figure 3(o), where the particles exhibited smoother surfaces, indicating full particle diffusion. In Figure 3(n) and Figure 3(o), where the scanning speed is 75 mm/s and 50 mm/s, respectively, the size of the joined particles was approximately three times the original size. This enlargement is due to neighbouring particles melting and diffusing together. It was observed that increasing the laser power and scanning speed increased neck formation. A significant increase in the neck growth ratio was observed during the early stages of neck development. However, as the particles approached a size of 100 µm, the growth rate of the neck began to slow. This behaviour can be explained by the Young-Laplace law, where the pressure difference influences neck growth in the molten material. According to Eq. (3), pressure is inversely proportional to the radius, meaning that as the radius decreases, the pressure difference increases. The Bernoulli principle further explains that a fluid will flow from areas of high pressure to areas of low pressure, thereby minimizing energy differences within the system.

$$\Delta P = \gamma \left(\frac{1}{R1} + \frac{1}{R2}\right) \tag{3}$$

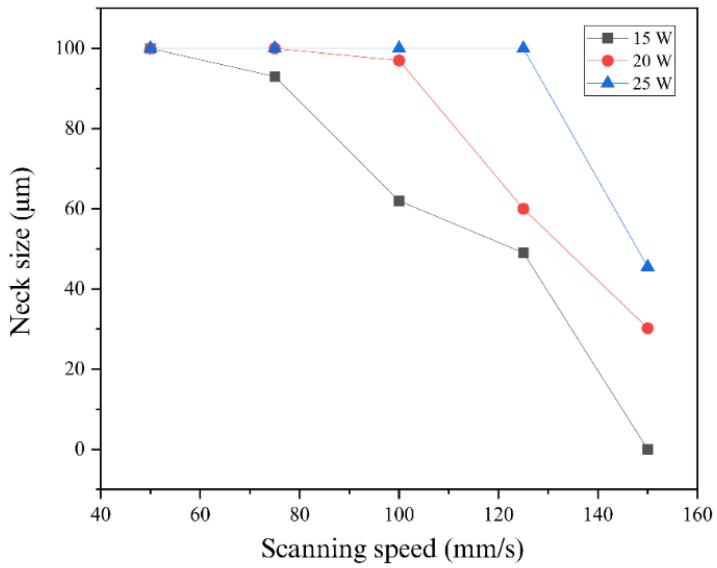

Figure 4. Trend graph of neck size versus scanning speed under different laser powers

As shown in Figure 5, the highest pressure is concentrated at the smallest radius, which is the neck area. Consequently, the molten material flows outward from the necking region to reduce the energy difference, leading to an increase in neck size between the particles. This phenomenon was demonstrated by Dai [19], who showed that the curvature at the contact zone is more pronounced during the initial stages of neck formation, resulting in a higher driving force for atomic diffusion. Consequently, larger particles exhibit more stable and sustained neck growth compared to smaller particles [20].

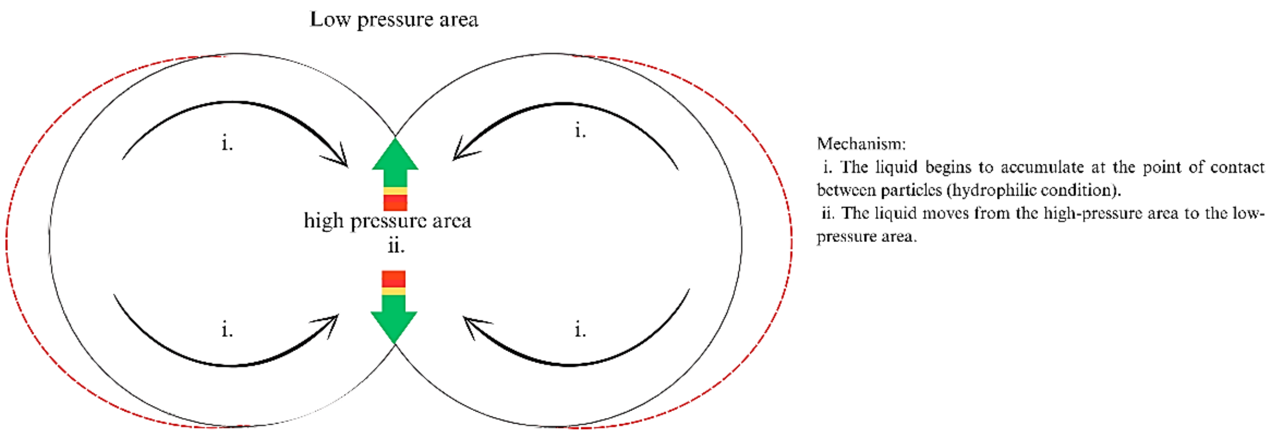

Figure 5. Schematic of liquid movement from a high-pressure area to a low-pressure area

3.2 Crystallographic Analysis

XRD analysis reveals that dislocation density increases as the scanning speed decreases, as shown in Figure 6. At 15 W and a scanning speed of 150 mm/s, the dislocation density is the lowest at 4.35×10^{13} m^{-2} indicating that no neck or plastic deformation occurred at this stage. As the scanning speed decreased to 125 mm/s, the dislocation density value increased to 6.96×10^{13} m^{-2}, corresponding to the formation of a small kink between particles, suggesting the onset of plastic deformation. The dislocation density continued to rise, reaching 7.11 $\times 10^{13}$ m^{-2} when the scanning speed was at 100 mm/s. At 75 mm/s the dislocation density was 7.62$\times 10^{13}$ m^{-2}, and 50 mm/s, the dislocation density is 8.71 $\times 10^{13}$ m^{-2}, indicating increased plastic deformation and neck formation. A similar trend was observed at 20 W and 25 W, where dislocation density increased as the energy density rose. At 150 mm/s and 20 W, the dislocation density was higher compared to 15 W, indicating that the initial neck formation had already begun at this stage. At 125 mm/s, with a neck size of 60 µm, the dislocation density reached 7.25 $\times$ 10^{13} m^{-2}. The dislocation density continued to increase to 7.83$\times 10^{13}$ m^{-2}, 9.43$\times 10^{13}$ m^{-2}, and 1.07$\times 10^{14}$ m^{-2} at scanning speeds of 100 mm/s, 75 mm/s, and 50 mm/s, respectively.

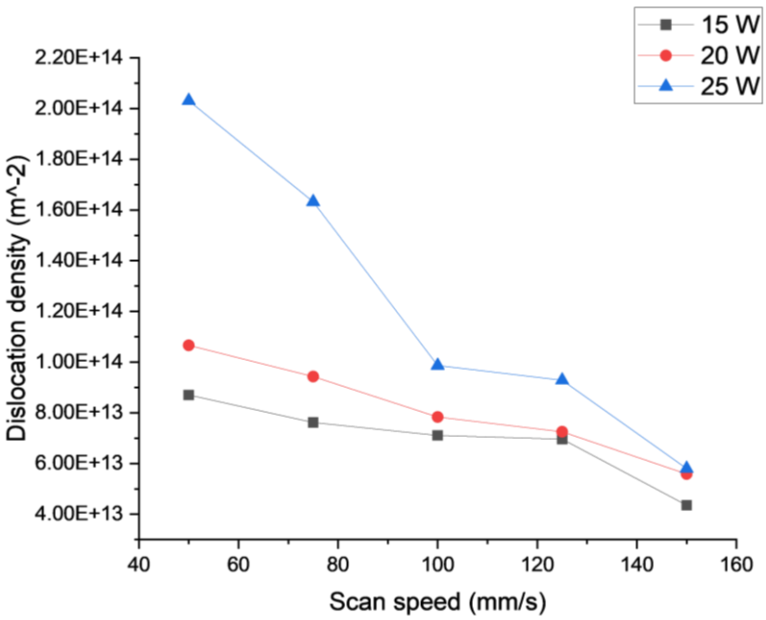

Figure 6. Effect of laser parameters on dislocation density

Meanwhile, at 25 W, a deviation from the trend was observed, as the particles fully diffuse at an early stage. At 150 mm/s, the dislocation density was 5.80 x10^{13} m^{-2}, indicating surface diffusion occurs at this stage. Only the outer surface of the atoms undergoes deformation processes. As the scanning speed decreased further, the dislocation density increased to 1.63 x10^{14} m^{-2} at 75 mm/s and 2.03 x10^{14} m^{-2} at 50 mm/s. This indicates that the particle size tripled, suggesting significant diffusion, particularly with neighboring particles. Typically, an increase in temperature results in a lower dislocation density [21]. This is because higher temperatures lead to longer cooling times, allowing the crystal structure more time to rearrange itself appropriately. However, the SLM process involves rapid solidification. When high energy density is applied, more heat is absorbed by the particles, allowing for greater atomic mobility and rearrangement. Due to the high-temperature gradients present during the SLM process, elongated grain structures are commonly observed. The rapid movement of atoms at elevated temperatures, combined with the limited time for atomic rearrangement or recovery, leads to an increased dislocation density in the as-built material [22].

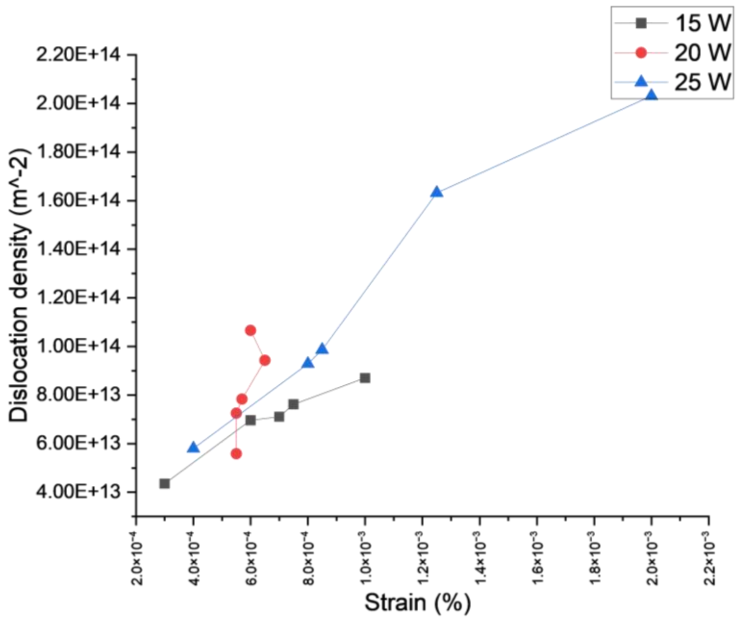

Figure 7. Relationship between dislocation density and strain under different laser parameters

The relationship between dislocation density and strain under different laser parameters is shown in Figure 7. In AM materials, the primary source of dislocation is deformation induced by thermal expansion and contraction in a constrained medium. When high heat energy is applied, it leads to plastic deformation, causing the lattice to undergo plastic strain [23]. As plastic deformation increases, strain also increases due to irreversible changes in the material, driven by dislocation movement, work hardening, and the activation of slip systems. A significant deviation can be observed at 25 W. When the dislocation density is below a critical threshold, the strength of the crystal is governed by the shear stress required to activate dislocation sources. As dislocation density increases, the likelihood of activating these sources rises, leading to a reduction in strength. However, once the dislocation density surpasses this threshold, shear strength becomes influenced by dislocation interactions. In this case, shear strength increases as dislocation density rises further, as these interactions inhibit dislocation motion [23-25]. In summary, this study offers insights into the mechanisms of neck formation during the additive manufacturing process and their role in particle bonding. While the current findings provide a foundation for understanding the early stages of material consolidation, the relationship between necking behavior and the formation of defects or mechanical performance remains to be thoroughly examined. Thus, detailed future investigations on mechanical testing and other microstructural characterization are required to verify these findings.

4. CONCLUSIONS

This study analyzes the effects of different laser powers and scanning speeds on neck formation in the SLM process. Therefore, the main results from this study are summarized and shown below;

i) When the laser power increases and the scanning speed decreases, the necking growth also increases. In this study, the highest necking growth occurs at a laser power of 25 W with a scanning speed of 50 mm/s. It has been found that the powder particles are fully dispersed, and their size is approximately triple their original size.
ii) When the neck size increases, the pressure gradient also decreases. Therefore, it led to a slower neck growth ratio.
iii) In this study, the dislocation density increases as the laser power or scanning speed decreases. The highest dislocation density value is 2.03 $x10^{14}$ m^{-2}, with the laser power of 25 W and the slowest scanning speed of 50 mm/s.

This study highlights the significance of understanding neck growth formation for the open SLM system. This understanding would facilitate the utilisation of a broader range of lasers capable of melting or sintering different types of materials and improve the production in SLM.

ACKNOWLEDGEMENTS

The authors acknowledge the financial support provided by the Ministry of Higher Education Malaysia (MOHE) under the Fundamental Research Grant Scheme (FRGS); FRGS/1/2020/TK0/UKM/03/5. The authors also appreciate the assistance provided by Universiti Kebangsaan Malaysia under the Dana Impak Perdana (DIP) scheme: DIP-2023-015.

CONFLICT OF INTEREST

The authors declare that they have no conflicts of interest.

AUTHORS CONTRIBUTION

M. R. Mazlan (Conceptualization; Investigation; Data curation; Writing - original draft; Resources)

N. H. Jamadon (Conceptualization; Formal analysis; Visualisation; Supervision, Reviewing manuscript)

A. B. Sulong (Project administration; Supervision)

F. I. Jamhari (Investigation; Data curation)

M. A. Aripin (Investigation; Data curation)

N. A. M. Radzuan (Supervision)

F. Yusof (Supervision)

AVAILABILITY OF DATA AND MATERIALS

The data supporting this study's findings are available on request from the corresponding author.

ETHICS STATEMENT

This research complies with the ethical guidelines of the National University of Malaysia. Since the study does not involve human participants, animals, or hazardous materials, no specific ethical approval was necessary.

REFERENCES

[1] B. DeBoer, N. Nguyen, F. Diba, A. Hosseini, "Additive, subtractive, and formative manufacturing of metal components: a life cycle assessment comparison," *International Journal of Advanced Manufacturing Technology*, vol. 115, no. 1–2, pp. 413–432, 2021.

[2] S. Pradhan, S. Singh, C. Prakash, G. Królczyk, A. Pramanik, C. I. Pruncu, "Investigation of machining characteristics of hard-to-machine Ti-6Al-4V-ELI alloy for biomedical applications," *Journal of Materials Research and Technology,* vol. 8, no. 5, pp. 4849–4862, 2019.

[3] A. Khatri, M. P. Jahan, "Investigating tool wear mechanisms in machining of Ti-6Al-4V in flood coolant, dry and MQL conditions," *Procedia Manufacturing*, vol. 26, pp. 434–445, 2018.

[4] F. M. Foudzi, L. Y. Hung, F. I. Jamhari, M. A. Buhairi, A. B. Sulong, N. Muhamad, et al., "Physical and hardness performance at different surfaces for titanium alloy (Ti6Al4V) printed using selective laser melting process (SLM)," *Jurnal Kejuruteraan*, vol. 36, no. 3, pp. 1217–1226, 2024.

[5] D. Herzog, V. Seyda, E. Wycisk, C. Emmelmann, "Additive manufacturing of metals," *Acta Materialia*, vol. 117, pp. 371–392, 2016.

[6] M. Bakhtiarian, H. Omidvar, A. Mashhuriazar, Z. Sajuri, C. H. Gur, "The effects of SLM process parameters on the relative density and hardness of austenitic stainless steel 316L," *Journal of Materials Research and Technology*, vol. 29, no. 1, pp. 1616–1629, 2024.

[7] T. Liu, Q. Wang, X. Cai, L. Pan, J. Li, Z. Zong, et al., "Effect of laser power on microstructures and properties of Al-4.82Mg-0.75Sc-0.49Mn-0.28Zr alloy fabricated by selective laser melting," *Journal of Materials Research and Technology*, vol. 18, pp. 3612–3625, 2022.

[8] F. I. Jamhari, F. M. Foudzi, M. A. Buhairi, A. B. Sulong, N. A. M. Radzuan, N. Muhamad, et al., "Influence of heat treatment parameters on microstructure and mechanical performance of titanium alloy in LPBF: A brief review," *Journal of Materials Research and Technology*, vol. 24, pp. 4091–4110, 2023.

[9] F. M. Foudzi, M. A. Buhairi, F. I. Jamhari, "Influence of processing parameters of selective laser melting (SLM) on additive manufactured titanium alloy (Ti6Al4V)," in *Proceedings of Mechanical Engineering Research Day*, pp. 55–57, 2020.

[10] M. R. Mazlan, N. H. Jamadon, M. A. Aripin, A. B. Sulong, A. M. Halil, M. Ishak, et al., "Effect of laser speed on neck formation in SS316L powder joining for LPBF," *Journal of Materials Research and Technology*, vol. 32, no. August, pp. 3382–3389, 2024.

[11] C. Pu, F. Liu, S. Wang, "Liquid force and rupture distance between two particles," *Advances in Materials Science and Engineering*, vol. 2021, pp. 1-9, 2021.

[12] S. Murali, D. P. Birnie, "Neck formation in reactive sintering: A model 2-D experiment," *Journal of Materials Research*, vol. 27, no. 8, pp. 1193–1197, 2012.

[13] F. Qin, Q. Shi, G. Zhou, X. Liu, L. Chen, W. Du, "Influence of powder particle size distribution on microstructure and mechanical properties of 17-4 PH stainless steel fabricated by selective laser melting," *Journal of Materials Research and Technology*, vol. 25, pp. 231-240, 2023.

[14] M. A. Buhairi, F. M Foudzi, F. I. Jamhari, A. B. Sulong, N. A. M. Radzuan, N. Muhamad, et al., "Review on volumetric energy density: influence on morphology and mechanical properties of Ti6Al4V manufactured via laser powder bed fusion," *Progress in Additive Manufacturing*, vol. 8, no. 2, pp. 265-283, 2022.

[15] M. R. Mazlan, N. H. Jamadon, A. Rajabi, A. B. Sulong, I. F. Mohamed, F. Yusof, et al., "Necking mechanism under various sintering process parameters – A review," *Journal of Materials Research and Technology*, vol. 23, no. 3, pp. 2189–2201, 2023.

[16] P. Hejmady, L. C. A. Van Breemen, P. D. Anderson, R. Cardinaels, "Laser sintering of polymer particle pairs studied by in situ visualization," *Soft Matter*, vol. 15, no. 6, pp. 1373–1387, 2019.

[17] J. Jhabvala, E. Boillat, R. Glardon, "Study of the inter-particle necks in selective laser sintering," *Rapid Prototyping Journal*, vol. 19, no. 2, pp. 111–117, 2013.

[18] N. Campos, T. Tinga, "Revealing the effects of powder reuse for selective laser melting by powder characterization," *The Journal of The Minerals, Metals & Materials Society*, vol. 71, no. 3, pp. 1062–1072, 2019.

[19] H. Dai, D. Chen, Z. Zheng, "Modelling the sintering neck growth process of metal fibers under the surface diffusion mechanism using the lattice boltzmann method," *Metals*, vol. 9, no. 5, p. 614, 2019.

[20] J. Zhang, D. Gu, Y. Yang, H. Zhang, H. Chen, D. Dai, et al., "Influence of particle size on laser absorption and scanning track formation mechanisms of pure tungsten powder during selective laser melting," *Engineering*, vol. 5, no. 4, pp. 736–745, 2019.

[21] N. Tabatabaei, A. Zarei-Hanzaki, A. Moshiri, H. R. Abedi, "The effect of heat treatment on the room and high temperature mechanical properties of AlSi10Mg alloy fabricated by selective laser melting," *Journal of Materials Research and Technology*, vol. 23, pp. 6039–6053, 2023.

[22] S. Gorsse, C. Hutchinson, M. Gouné, R. Banerjee, "Additive manufacturing of metals: a brief review of the characteristic microstructures and properties of steels, Ti-6Al-4V and high-entropy alloys," *Science and Technology of Advanced Materials*, vol. 18, no. 1, pp. 584–610, 2017.

[23] Y. Yu, M. Zu, C. Ren, W. Zhang, "Effect of strain rate on the plastic deformation and fracture of 90W-7Ni-3Fe alloy prepared by liquid-phase sintering," *Journal of Materials Engineering and Performance,* vol. 27, no. 12, pp. 6606–6615, 2018.

[24] J. A. El-Awady, "Unravelling the physics of size-dependent dislocation-mediated plasticity," *Nature Communications*, vol. 6, pp. 1–9, 2015.

[25] W. Zhou, X. Ren, Y. Yang, Z. Tong, L. Chen, "Dislocation behavior in nickel and iron during laser shock-induced plastic deformation," *International Journal of Advanced Manufacturing Technology,* vol. 108, no. 4, pp. 1073–1083, 2020.